A novel inflation adhesion test for elastomeric matrix / steel cord

K. Kane, J. Jumel, F. Lallet, A. Mbiakop-Ngassa, J.-M. Vacherand, M.E.R. Shanahan

A Novel Inflation Adhesion Test for Elastomeric Matrix / Steel Cord

K. Kane[1,4], J. Jumel[*,1,2,3], F. Lallet[4], A. Mbiakop-Ngassa[4], J.-M. Vacherand[4], M.E.R. Shanahan[1,2,3]

[1]University of Bordeaux, I2M, UMR 5295, F-33400 Talence, France.

[2]CNRS, I2M, UMR 5295, F-33400 Talence, France.

[3]Arts et Métiers Paris Tech, I2M, UMR 5295, F-33400 Talence, France.

[4]Manufacture française des pneumatiques MICHELIN, Site de Ladoux, 23 place Carmes Déchaux, 63040 Clermont-Ferrand, France.

Abstract:

A novel test configuration is proposed to characterize the adhesion between an elastomeric matrix and an included steel cord. The circular cylindrical, rubber envelope is bonded to the cord along the axis of symmetry. A crack is forced to propagate along the interface by inflating the rubber envelope using a pressurised liquid in between the two media. The constant pressure recorded during the test is used to evaluate the interfacial critical strain energy release rate (Critical SERR). This is achieved using an analytical model, taking into account both the incompressible, hyperelastic nature of the rubber and geometrical nonlinearity due to large deformations. An energy balance is proposed to evaluate the interfacial SERR.

Keywords:

Rubber cord adhesion, hyperelasticity, inflation test.

[*] Corresponding author: Julien Jumel, julien.jumel@u-bordeaux.fr

Nomenclature

v_0, w_0 : inner, outer initial rubber enveloppe radius, undeformed state

v, w : inner, outer rubber enveloppe radius, deformed state

R : inner radius of the confinement tube

λ_r, λ_θ, λ_z : radial, circumferential and axial rubber elongation

r, r_0 : radial position, deformed / initial configuration

c, d : integration constants

p : hydrostatic pressure stress component

C_1, C_2 : Mooney Rivlin behaviour constants

σ_r, σ_θ, σ_z : radial, circumferential and axial component of the stress tensor

$\alpha = C_2/C_1$: dimensionless parameter

$h = w_0/v_0$: dimensionless parameter

$K = 1/ca^2$: dimensionless parameter

P_i : Internal inflation pressure

$P_{n=} P_i/2C_1$: Dimensionless internal inflation pressure

UIS : Unconfined Inflation Stage

CIS : Confined Inflation Stage

G, Gc : Strain Energy Release Rate (SERR), critical SERR

1. Introduction

Tyres are complex multi-layered structures, which maintain the contact between vehicle and soil. Their tribological and mechanical performances are therefore crucial. In addition, for safety and reliability reasons, durability is still an issue since tyres must sustain severe in-service loading conditions as well as aggressive environmental exposure. Their structure mostly consists of rubber layers reinforced with textile or metal cords, which control the overall stiffness as well as the strength of the structure (Lechtenboehmer A.). As it is in all composite structures, mastering the matrix (rubber) to reinforcement (cord) adhesion is very crucial. The most traditional technique to ensure strong chemical adhesion between metal cord and rubber consists of depositing a thin layer of brass on steel wires before embedding them in the raw (un-vulcanized) rubber. During the vulcanization process, Cu_xS bonds are produced (van Ooij) which develop strong chemical links between the two materials. However, this adhesive interface suffers from progressive degradation due to water diffusion that provokes corrosion of the interface (Stevenson A.). Therefore, new coatings having better adhesive and ageing behaviour are under development. In this context, the development of refined experimental characterization procedures to evaluate the mechanical performances of the interface is an issue since the mechanical properties are generally evaluated with standard procedures whose result may suffer from various experimental artefacts.

To evaluate the adhesion between layers, peel tests are generally used such as (Cook J. W.), (D1781-98(2012)), (D1871-04(2014)), (D2229-10(2014)) & (D429-14). Such tests are also used for testing new coating performance but are applicable only in planar configuration. Brass coating is generally deposited on the steel during the final humid drawing step of the cords. This specific process will confer to the coating a specific structure in terms of roughness, homogeneity, grain size and so on (Rault V.), (Vignal V.), (Zelin M.). As a consequence, using peel test for characterizing rubber adhesion on plated plate could lead to

biased results especially if other deposition methods are used such as electroplating, PVD or else." .

Apart from the classical peel test protocol, other standardized procedures are proposed to evaluate rubber adhesion to rigid substrate (ISO 5600 : 2011 – rubber – determination of adhesion to rigid materials using conical shaped parts) ensuring crack propagation along the interface.

Other specialized test protocols and specimens have also been proposed in the literature (Brown R.) for better observation and evaluation of crack propagation conditions. Despite more homogeneous and better controlled loading conditions, plane geometries are used again which are not compatible with cord-rubber adhesion evaluation. In these works (Brown R.), advanced fracture mechanics is proposed to evaluate the mode mixity condition at the crack tip so as to evaluate the influence of the material viscosity.

For a better evaluation of the cord-rubber adhesion, testing for individual cord -rubber mechanical behaviour is fundamental. The pull-out test, as describe in the ASTM standard (D1871-04(2014)), (Jamshidi M.) & (Gent A.N.), is generally used for that purpose. Although this test is simple to implement, quantitative evaluation of adhesive performances is difficult to achieve. Since the failure of the specimen is controlled by many parameters (wire / rubber plasticity, interface failure, mode mixing and so on) as well as artefacts (interface friction, tools friction). In order to achieve more intrinsic evaluation of mechanical performances of cord/rubber adhesive system a new test configuration is proposed here. The protocol is inspired by the more traditional blister test (Dannenberg H.), which is used to evaluate the adhesive properties of coating or painting. The test commences with injecting a pressurized fluid between the substrate and the coating aimed at fracturing the interface; the SERR can therefore be determined by monitoring both the crack extension as well as the pressure evolution during the test. Such protocol has also been used for characterizing rubber/substrate

4

adhesion in planar configuration (Dillard D. A.). In such blister tests however, a coating failure was generally observed due to strong adhesion. Therefore, to prevent the failure of the coating layer, a confinement system is used (Napolitano M.J.), (Chang Y. S.) & (Parsons M.). To evaluate rubber / cord adhesion, a cylindrical version of the constrained blister test is proposed here. The test specimen consists of a cylindrical rubber envelope partially bonded to a metal wire along its central axis. A crack is forced to propagate along the interface by injecting a liquid under pressure in between the two media from the debonded side, as shown in *Figure 1*. A concentric confinement envelope is used outside the rubber cylinder to prevent unstable inflation (and therefore unstable failure). A constant pressure value is recorded during the crack propagation associated to self-similar crack propagation process which can be used to evaluate the interface critical SERR.

Inflation of a thick hyperelastic cylinder has been studied for a Neo-Hookean material by (Anani Y.). However, the type of rubber material provided by Michelin was a Mooney-Rivlin solid (Mooney M.). The Mooney-Rivlin constants were also provided along with the specimens. The scope of this work was to develop a successful test setup and formulate a theoretical as well as an analytical model that describes the tests. The detailed analysis of material properties is left for future research prospects.

In this article, the test set-up is described with preliminary experimental results. Subsequently, a thick hyperelastic cylinder inflation model is developed based on Skala's (Skala D. P.) work, to evaluate the effect of fluid pressure on rubber envelope deformation. Therefore . The analytical model is compared with a FE model for verification of the obtained results. Finally, a global energy balance is performed for quantitative evaluation of the interface SERR from various measurable properties (fluid injection pressure, specimen geometry and deformation, material properties).

2. Rubber cord adhesion inflation test – RCAIT

Prior to the development of the theoretical and numerical modelling of the problem, an experimental test campaign was conducted to validate the experimental protocol. In the following sections, details of the test and the presentation of representative results are presented also to indicate pressure range in the present configuration.
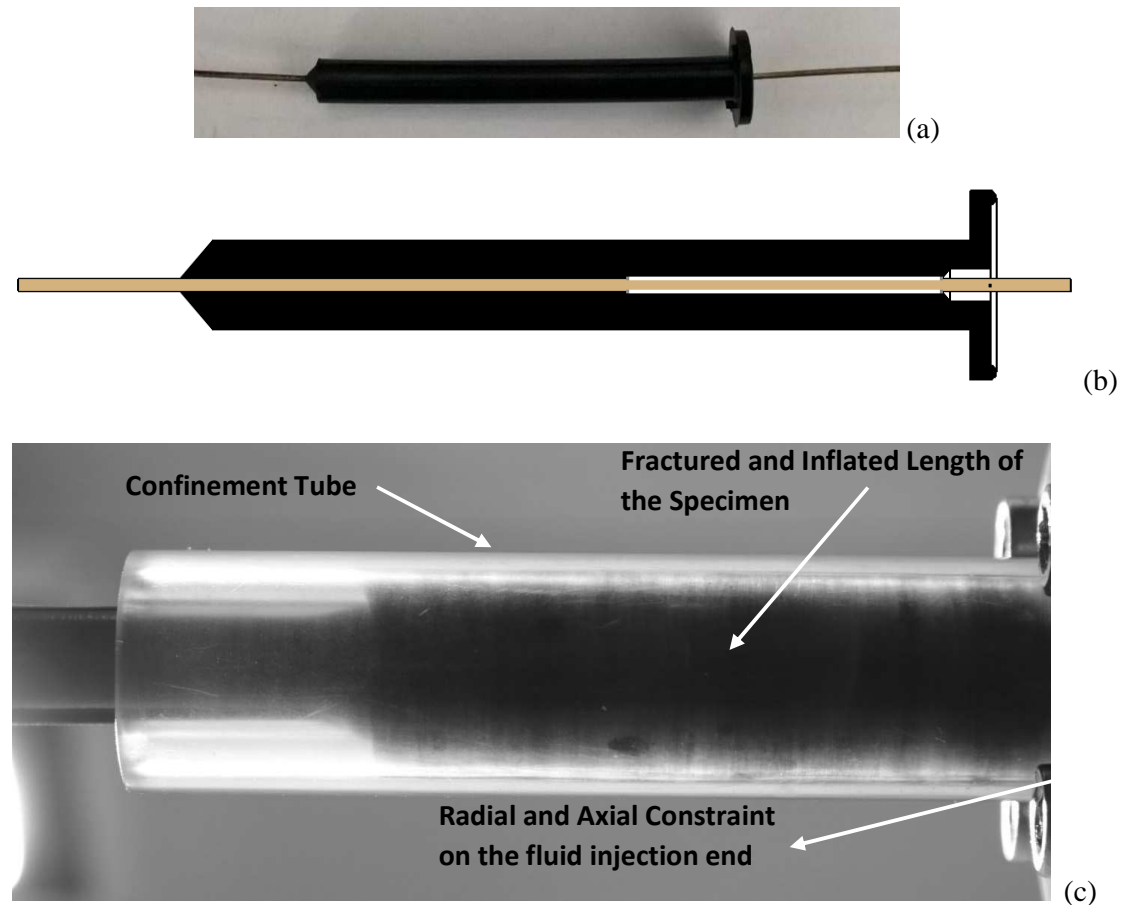

(a)

(b)

(c)

Figure 1. (a) Test Specimen (b) Schematic of the specimen cross-section. The initial debonding length is shown as a white tape on the steel cord. (c) Inflated specimen during the test. The 'fractured and inflated' length of the rubber envelope is touching the PMMA confinement tube.

2.1. Experimental set-up

The test specimen, presented in *Figure 1*, consists of a $\phi=1.3mm$ steel wire coated with brass. The steel wire is embedded axially in a $\phi=9.4mm$ cylindrical rubber envelope. The initial crack or debonding is created by applying a PTFE tape on a length of *50mm* on the steel cord from the fluid injection side, before the vulcanization process. The vulcanization process bonds the rest of the steel cord to the rubber, leaving an initial crack length of *50mm*. Prior testing, the specimen is placed in a climatic chamber and exposed to 40°C and 60%RH atmosphere for 60 hours to simulate accelerated ageing conditions. After the ageing process, the specimen is tightened to the test bench at its fluid injection end imposing radial and axial constrain. While doing so, the rubber envelope is held fixed only while the steel cord is free to move axially during the test, allowing the debonded rubber length to inflate freely. A PMMA tube with *10mm* internal diameter and *5mm* thickness is used for radial confinement of the specimen. To provoke interface separation, demineralised water is injected at *2ml/min* using a *KD Scientific 410 Series* syringe pump equipped with a 20ml syringe. During the experiment, the pressure is recorded using *Swagelok S Model Transducer* with a capacity of 250bar.

2.2. Experimental Results

Figure 2(a) shows the evolution of pressure versus injected water volume during the test. The test sequence is divided into two phases. Up to approx. *5ml*, the pressure is increasing while the water is injected in the rubber envelope. No crack propagation is observed during this phase; but the envelope is visibly inflated and can be seen touching the confinement tube. After nearly *8ml* of fluid injection, a pressure of approx. *66.6 bar* is recorded followed by a steady increase in the inflated length of the specimen that corresponds to the crack propagation. Nearly constant pressure is observed during the crack propagation,

corresponding to a nearly constant Strain Energy Release Rate, similar to the study by (Chang Y. S.).
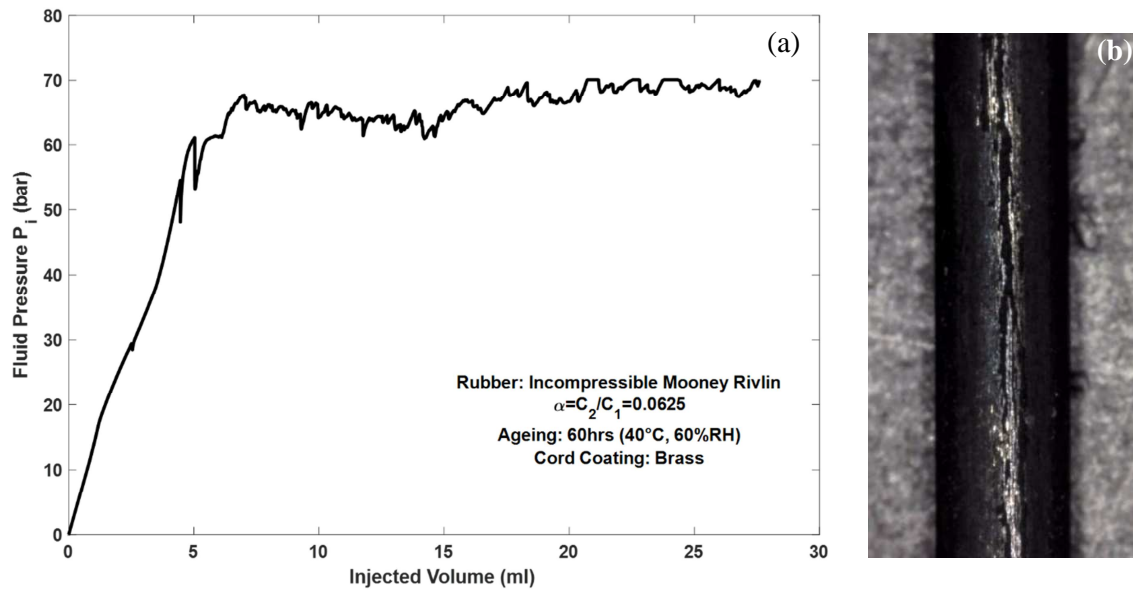

Figure 2: (a) Fluid Pressure vs Injected Volume. A nearly constant fluid pressure is observed during the crack propagation stage (approx. 8ml)), (b) Fracture surface of the steel cord. The shining spots (brass-coated steel) indicate an adhesive failure.

After the test, the rubber envelope is cut open to observe the cord crack face. Adhesion failure is observed since no remaining rubber is observed on the wire surface. The brass-coated steel can be seen shining on the crack face in *Figure 2 (b)*.

3. Thick rubber tube inflation model

We now consider a thick elastomer envelope or tube under internal pressure as previously studied by (Skala D. P.). The main notations, results and constitutive equations are recalled below before some modification of the boundary conditions are considered to take into account the effect of radial confinement. With these mathematical derivations, we aim to

describe the stress state in the rubber envelope of the specimen as well as the strain energy stored considering its incompressible hyperelastic nature. Ultimately, an energy balance analysis of the water injection process is proposed to determine the Strain Energy Release Rate associated with the crack propagation.

3.1. Constitutive equations

We consider a thick hollow elastomer tube with inner and outer radii given by v_0 and w_0 respectively. The problem to solve is clearly axisymmetric, therefore only radial and axial displacements are considered here. The radial and circumferential principal stretch ratios are given by:

$$\lambda_r = \frac{dr}{dr_0} \qquad\qquad \lambda_\theta = \frac{r}{r_0} \qquad\qquad (1)$$
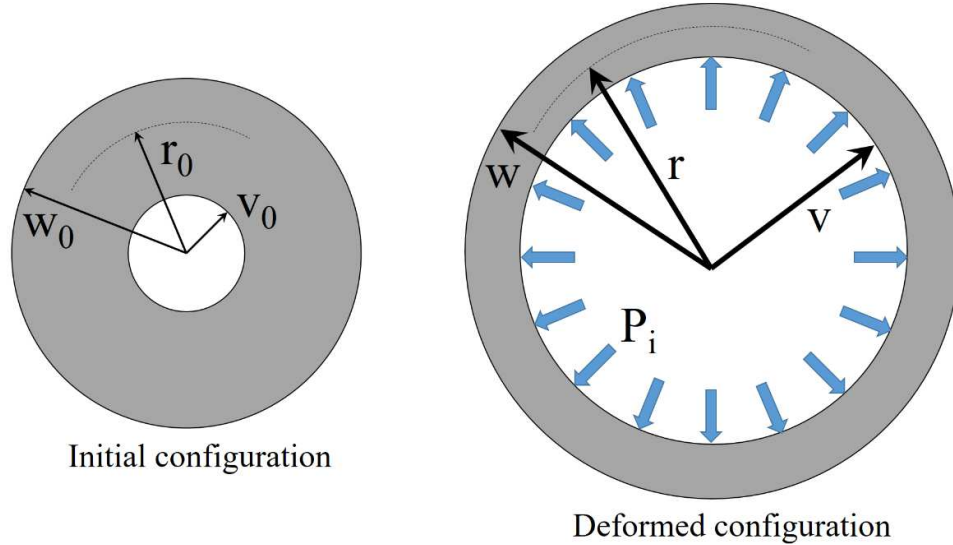

Figure 3: Rubber tube deformation stages. P_i is the applied fluid pressure.

r_0 and r being the radial position in the initial state and deformed state respectively. Taking into account the incompressible nature of the material with relation $\lambda_r \lambda_\theta \lambda_z = 1$, and considering a constant through-thickness axial stretch, the general expressions of radial and circumferential stretch ratio in an axisymmetric configuration are found (Skala D. P.):

$$\lambda_r^{\,2} = \lambda_z^{\,-1}\left[1 - \frac{1}{cr^2}\right] \qquad\qquad \lambda_\theta^{\,2} = \lambda_z^{\,-1}\left[\frac{cr^2}{cr^2 - 1}\right] \qquad\qquad (2)$$

with c being an integration constant to be determined from constitutive and boundary condition equations together with λ_z. The general expression of stretch ratios being known, we now assume an incompressible hyperelastic Mooney-Rivlin material behaviour (Mooney M.) for the rubber. This assumption is owing to the material data provided by Michelin, as explained earlier. Such behaviour is suitable for a hyperelastic material when deformation does not exceed 200%. The relation between Cauchy Stresses and stretch ratios is given by:

$$\sigma_i = 2C_1 \lambda_i^2 - 2C_2 \lambda_i^{-2} + p \qquad\qquad (3)$$

p being the local hydrostatic pressure component of stresses. Under axisymmetric loading condition, the equilibrium equation gives the relation:

$$\frac{d\sigma_r}{dr} + \frac{\sigma_r - \sigma_\theta}{r} = 0 \qquad\qquad (4)$$

Combining equations *(2)*, *(3)* and *(4)* according to the procedure followed by (Skala D. P.), a general expression of the hydrostatic pressure component, p, is found:

$$\frac{p}{2C_1} = \left\{ \frac{1}{cr^2} - \ln\left(\frac{cr^2}{cr^2 - 1}\right) \right\} \frac{1}{2\lambda_z} - \left\{ \frac{1}{2cr^2} + \frac{1}{2}\ln\left(\frac{cr^2}{cr^2 - 1}\right) - \frac{1}{cr^2 - 1} \right\} \alpha\lambda_z + d \qquad (5)$$

with $\alpha = C_2/C_1$. Therefore, the stress distribution in the rubber is fully determined by only three parameters λ_z, c and d, which are obtained by solving the boundary condition equations as described hereafter.

3.2. Boundary conditions

Two different sets of boundary conditions should be considered since two phases are observed during the inflation test. Initially, the outer surface of the rubber envelope is free to expand since there is no contact with the confinement tube. This phase is called Unconfined Inflation Stage (UIS). The following set of boundary conditions is therefore considered.

$$\sigma_r(r = v) = -P_i \qquad (6)$$

$$\sigma_r(r = w) = 0 \qquad (7)$$

$$\int_v^w \sigma_z(r)2\pi r dr = P_i\pi v^2 \qquad (8)$$

P_i is the fluid pressure imparted by the injected water. The cord immersed in the pressurized fluid is not clamped and can move axially freely. Therefore, the axial force applied to the rubber envelope is given by equation (8).

11

The detailed explanations for the rest of the boundary conditions can be found in Skala's original article (Skala D. P.). Solving the boundary conditions as simultaneous equations, and defining the two dimensionless quantities $h = w_0/v_0$ and $K = 1/(cv_0^2)$, a transcendental relation is found:

$$-2(h^2 - 1)\left(\lambda_z^3 - 1 + \alpha\lambda_z^2 - \frac{\alpha}{\lambda_z}\right) + K\lambda_z(1 - \alpha\lambda_z^2)ln\left[\frac{h^2(1 + K\lambda_z)}{h^2 + K\lambda_z}\right] = 0 \qquad (9)$$

This relation is solved numerically to determine the K versus λ_z evolution from which all stretch ratios and stresses can be found w.r.t. the dimensionless pressure P_n $(= P_i/2C_1)$ using
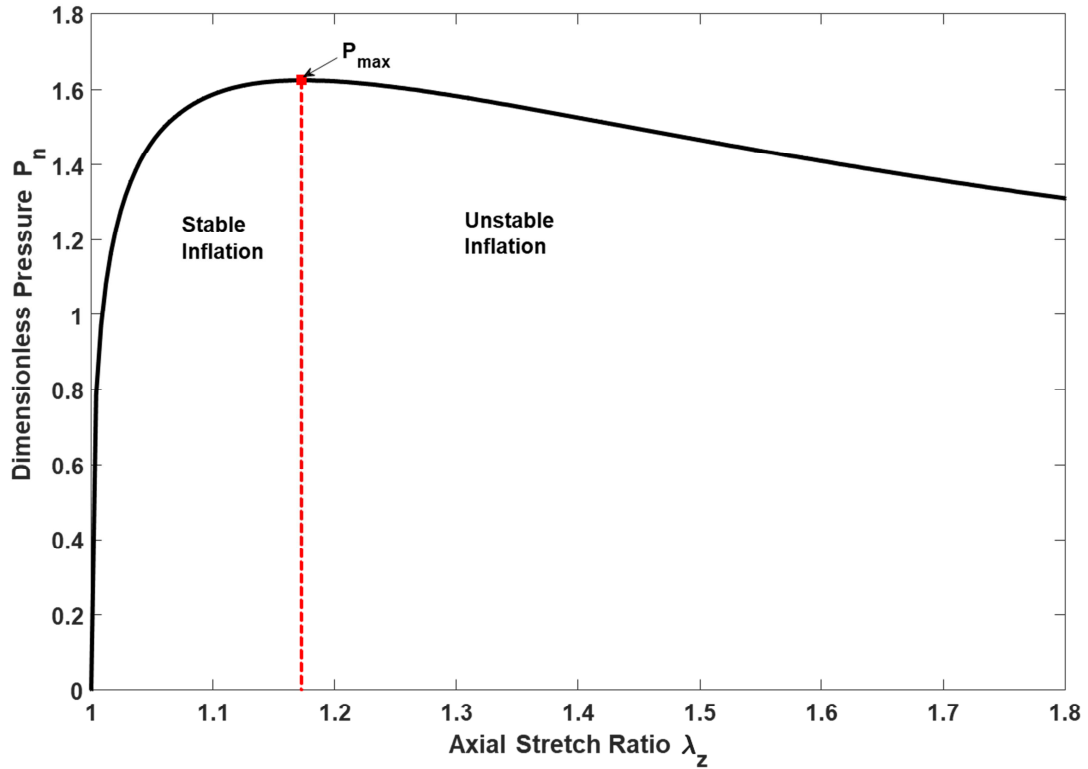
equations *(2)* to *(5)*.

Figure 4: Unstable inflation of rubber cylinders. P_{max} is the maximum fluid pressure and the point of instability.

The unconfined cylindrical inflation tests are known to be susceptible to instabilities which should be avoided to keep the present analysis valid (Gent A. N.), see *Figure 4*. Inflating the cylinder past the instability point P_{max} is an unstable condition, making the weak regions in the rubber envelope susceptible to fracture. In order to avoid fracture of the rubber envelope under high pressure and to ensure the metal / rubber interface separation, a confinement tube is used which prevents from any excessive deformation of the envelope as proposed by (Napolitano M.J.) in planar configuration for the blister test. The radial clearance between the undeformed rubber envelope and the confinement tube is small enough to ensure that the rubber envelope will touch the confinement before reaching the point P_{max} in *Figure 4*. This is the second phase of the inflation, which is called the Confined Inflation Stage (CIS). It is now important to alter the boundary conditions, which describes the transition from UIS to CIS.

The confinement envelope is supposed to be rigid therefore the outer radius of the rubber envelope remains constant. Hence, for the second set of boundary conditions, *(7)* is changed to:

$$w = R \tag{10}$$

With R being the inner radius of the confinement tube. Boundary conditions *(6)* and *(8)* remain the same for CIS. *Equation (10)* leads to the relation (see *Equation* (25) in (Skala D. P.) for intermediate steps):

$$R^2 = \frac{1}{c} + \frac{w_0{}^2}{\lambda_z} \tag{11}$$

Therefore, the constant c is determined directly as a function of the longitudinal elongation λ_z, with the relation:

$$c = \frac{\lambda_z}{\lambda_z R^2 - w_0^2} \qquad (12)$$

Similar to the UIS, integration of boundary condition equations *(6)*, *(8)* and *(10)* lead respectively to relations:

$$P_n = -\frac{1}{2\lambda_z}\left\{\frac{2 + K\lambda_z}{1 + K\lambda_z} - ln(1 + K\lambda_z)\right\} + \alpha\lambda_z\left\{\frac{3 + 2K\lambda_z}{2(1 + K\lambda_z)} + \frac{1}{2}ln(1 + K\lambda_z)\right\} - d \qquad (13)$$

$$(1 + K\lambda_z)P_n = \left(\lambda_z{}^2 - \frac{\alpha}{\lambda_z{}^2} + d\right)(h^2 - 1) + \frac{1}{2}K\lambda_z\left(\frac{1}{\lambda_z} - \alpha\lambda_z\right)ln\left(\frac{1}{h^2}\frac{h^2 + K\lambda_z}{1 + K\lambda_z}\right)$$

$$- \frac{1}{2}\left(\frac{1}{\lambda_z} + \alpha\lambda_z\right)([h^2 + K\lambda_z]ln[h^2 + K\lambda_z] - [1 + K\lambda_z]ln[1 + K\lambda_z]) \qquad (14)$$

with $P_n = P_i/2C_1$ being the dimensionless pressure. These two simultaneous non-linear equations can be solved numerically for a given value of λ_z. Finally, all displacements, stresses and stretch ratios are derived.

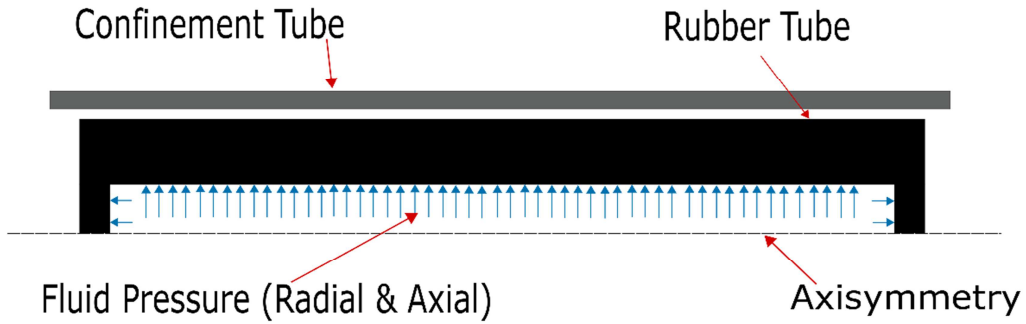### 3.3. Numerical Modelling

Figure 5: Schematic of the Rubber Cylinder Inflation modelled in ABAQUS.

The rubber cylinder inflation test was modelled in ABAQUS using the axisymmetric elements – CAX4RH and considering Mooney-Rivlin material behaviour and contact condition with a rigid confinement envelope (*Figure 5*). The mesh size gradually increased from the inner radius to the outer radius; *0.02mm* at the inner radius (v_0) and *0.1mm* at the outer radius (w_0). A confinement ratio (R/w_0) of *1.06* was chosen as in the experimental conditions. The rubber cylinder was modelled to be of a length of *500mm* and the displacements and stresses were calculated at the middle of the length to avoid any edge effects. *Figure 6* shows the comparative results of the inflation tests during the UIS and CIS with a confinement ratio of *1.06*. The UIS (black curve) and CIS (blue curve) are respectively, solutions to the *Equation (9)* and *Equation (13)-(14)*. After the *Confinement Contact* point, UIS follows unstable inflation whereas CIS follows stable inflation. Due to the instability condition after the point P_{max}, the numerical simulation (FE model) stopped as maximum pressure is reached. For the confined configuration with contact, the theoretical model is found to be in very good agreement with the FE model. The transition between the two stages is well captured.
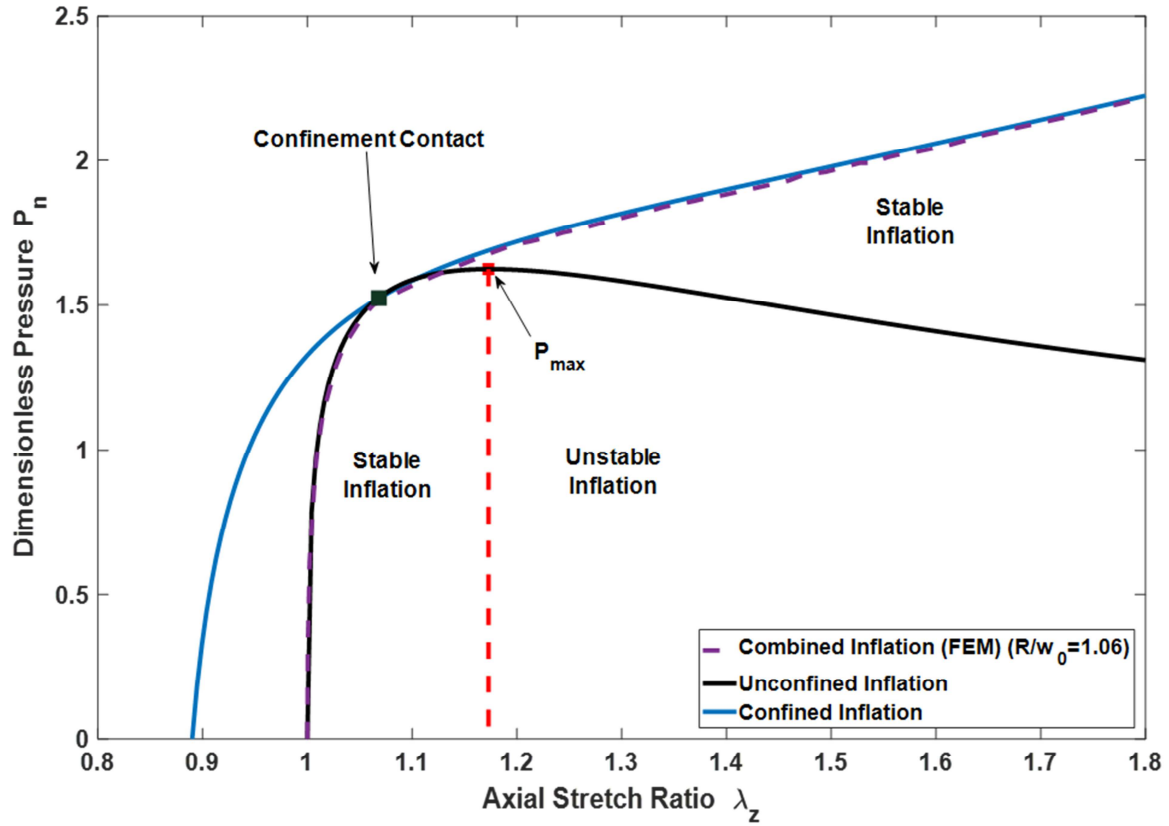
Figure 6: Comparison of Unstable and Stable inflation of the rubber envelope. Confinement contact comes prior to the point P_{max} thereby avoiding the instability. Results from the FEM simulation closely matches the theoretical model.

Once the analytical model is assessed, parametric investigation is performed. In particular, *Figure 7* illustrates the effect of the dimensionless rubber envelope radius h and confinement ratio R/w_0 on the rubber tube inflation. The overall response is the same whatever geometrical parameters are chosen. Obviously, the $P_n(\lambda_z)$ evolution does not depend on parameter R/w0 during the UIS and the specimen is found stiffer when h increases leading to higher P_n values. More interestingly, the dotted lines indicate the transition from UIS to CIS. It can be observed that there is a risk of unstable inflation and necking for large R/w_0 values since large λ_z values are needed to achieve contact condition in that case.
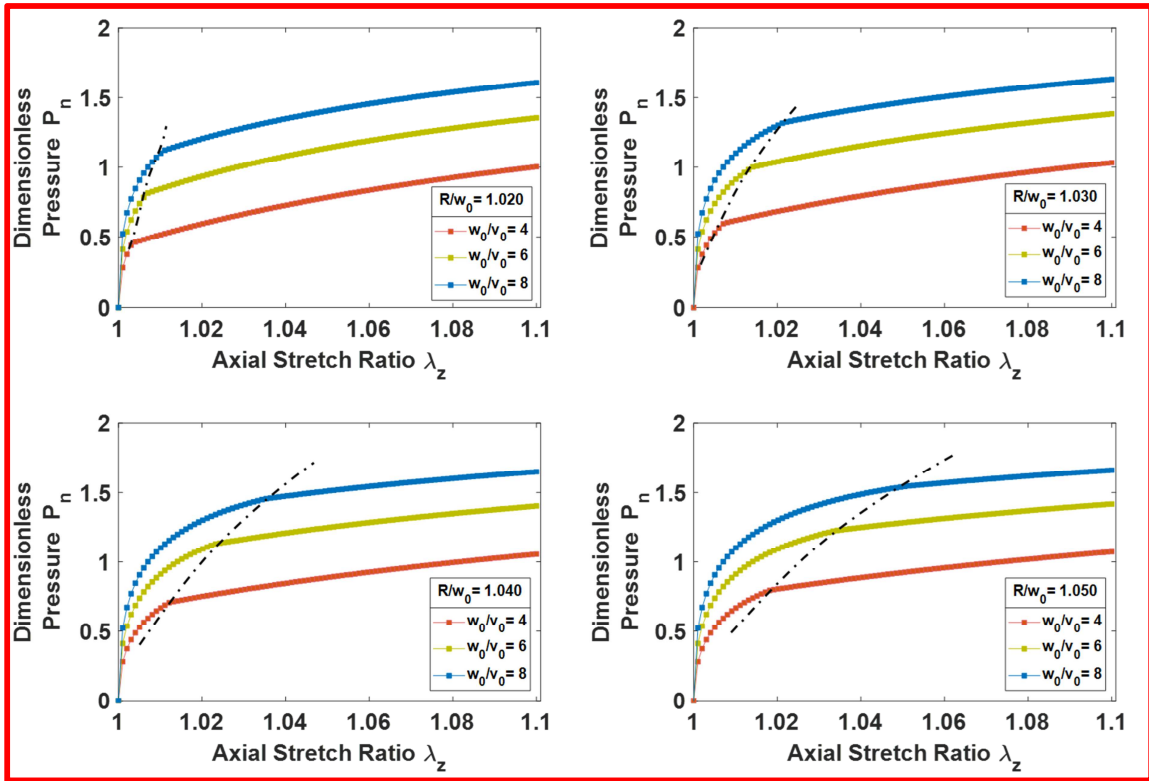
Figure 7: Effect of dimensionless radius ($h = w_0/v_0$) and confinement ratio (R/w_0) on Rubber Tube Inflation. Dotted lines represent confinement contact.

Similar plot for a constant dimensionless radius ($h=8$) and varying confinement ratios is shown in *Figure 8*. The confinement contact is highly sensitive to the confinement ratio. A slightly higher confinement ratio (>1.1) results into Unstable Inflation.
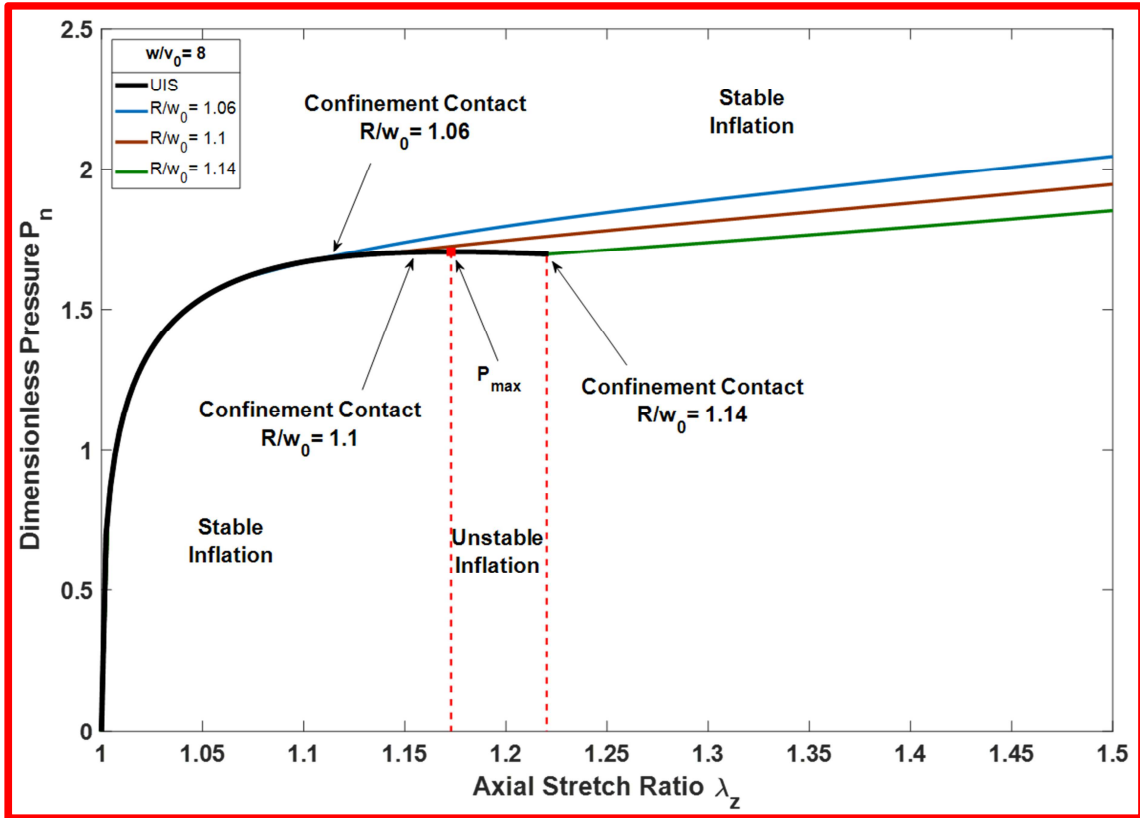
Figure 8: Effect of confinement ratio (R/w_0) on Rubber Tube Inflation for a fixed dimensionless radius (h = w_0/v_0=8).

3.4. Influence of boundary conditions

The Thick Rubber Tube Inflation Theory explained earlier is based on an important assumption that the Cauchy Stresses along the tube radius are not constant. This assumption is similar to the one in the standard Thick Cylinder Inflation Theory for elastic materials. For elastic materials, only Engineering (or Nominal) Stresses are calculated. However, for a hyperelastic material, the Cauchy Stresses are calculated due to the large deformations and displacements values that lead to geometrical nonlinearities. In this section, the stress variation along the rubber tube thickness owing to the various boundary conditions is studied. Effect of axial stretch ratio (λ_z) on the Cauchy Stresses as well as the Dimensionless Pressure (P_n) is elaborated.

In the previous analysis, a series of dimensionless parameters have been introduced which should be reminded here. $\alpha = C_2/C_1$ is a material parameter, defined for a Mooney-Rivlin solid. In this theoretical work, the same value of $\alpha = 0.0625$ which represents the specimen rubber material is used. The dimensionless pressure Pn is considered here as the driving quantity. All stress/stretch evolutions depend on the initial tube dimension as given by the
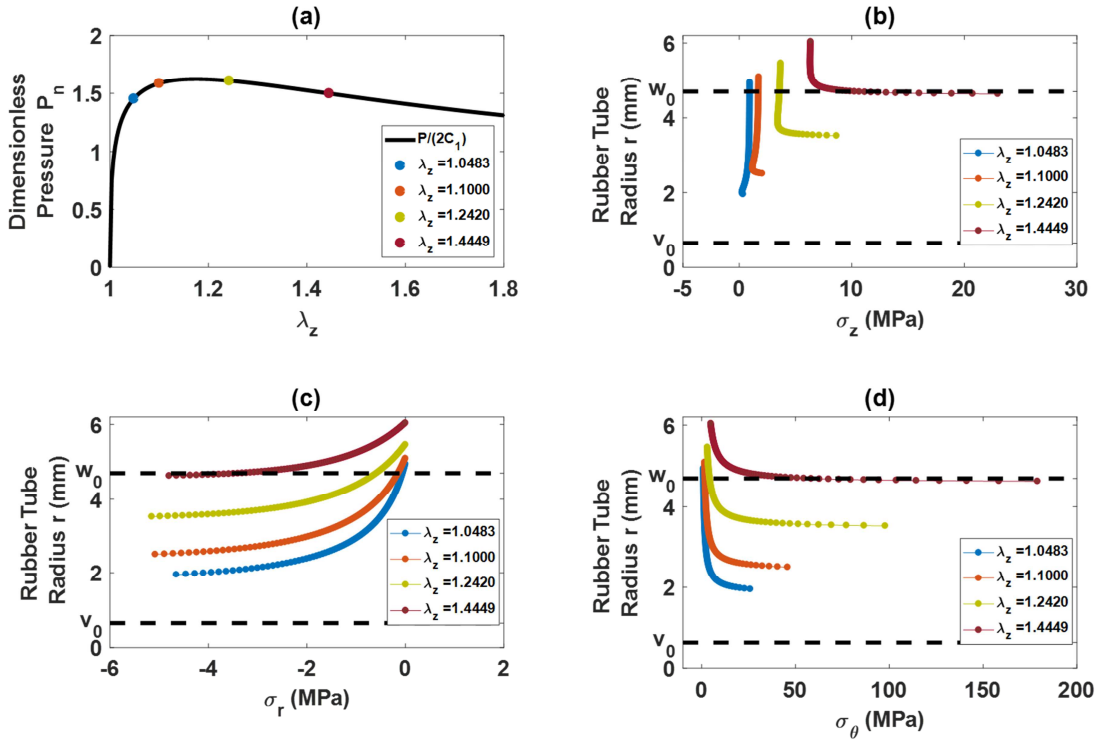

dimensionless radius, $h = w0/v0$.

Figure 9: Unconfined Inflation Test. Effect of Axial Stretch Ratios on Cauchy Stresses and P_n

For the UIS (R→∞), the Cauchy stresses are plotted as the abscissa with the deformed rubber tube radius as ordinate in Figure 8. Although confinement is absent, a decrease in the rubber tube thickness is observed with an increase in the axial stretch ratio λ_z, due to the incompressibility of the rubber. The horizontal dotted lines in *(b)*, *(c)*, and *(d)* represent the undeformed tube radii (w_0 and v_0). As the inflation enters the unstable region as shown in *Figure 4*, Cauchy Stresses σ_z and σ_θ increase dramatically. A significant variation of σ_r

across the tube thickness arises due to the significant thickness of the tube. A thin cylinder tube theory will fail to represent this result. The Cauchy Stress values need to be considered
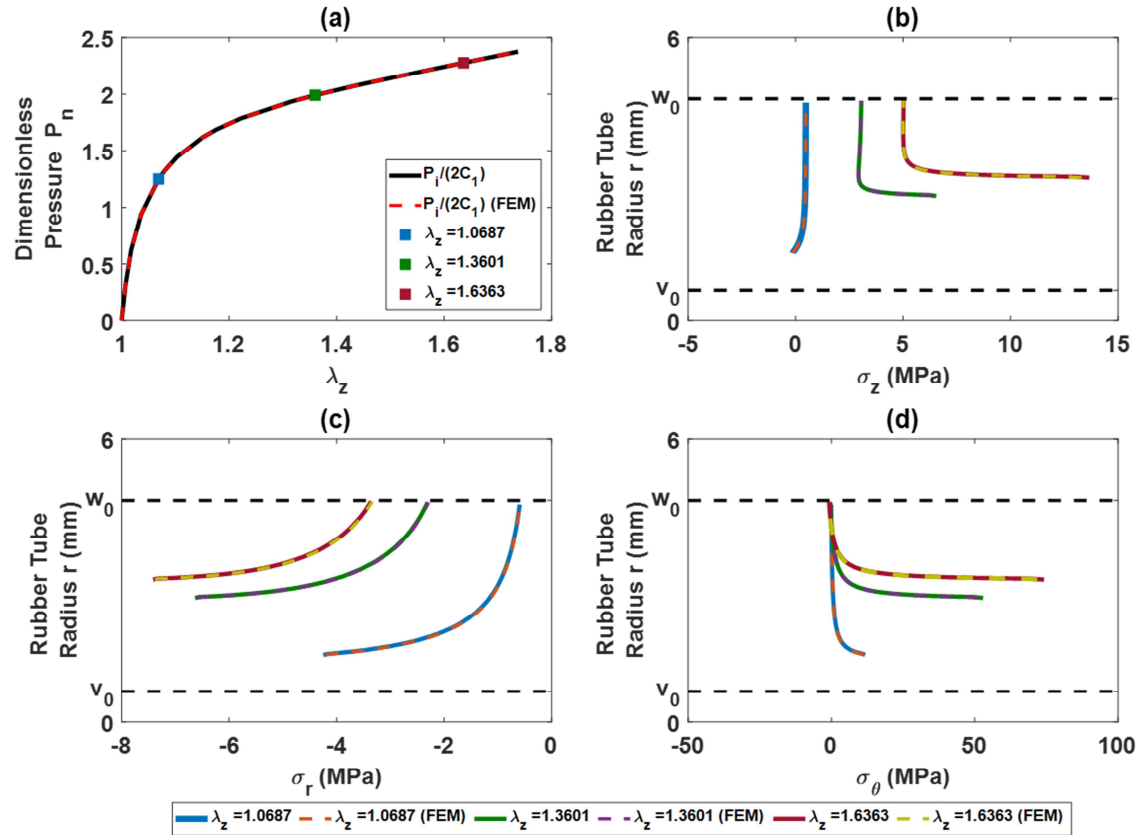
Figure 10: Purely Confined Inflation Test. Effect of Axial Stretch Ratios on Cauchy Stresses and P_n.

Similar plots can also be obtained in CIS ($w_0=w=R$). A comparison of the theoretical Cauchy Stress variation and the one from the FE model is shown in *Figure 10*. The stress variation at different axial stretch ratios is nearly identical for both methods of calculation. The horizontal dotted lines represent the undeformed tube radii (w_0 and v_0). The confinement tube is loaded with a radial pressure σ_r during the inflation. This σ_r is far from being negligible and possible radial expansion of the confinement tube could be expected in case this envelope would not be thick enough.

Despite the contact pressure, no frictional forces are expected since once the contact condition is reached between rubber and confinement envelope; no relative displacement is expected if the inner pressure remains constant. This might not be the case if large pressure fluctuations are measured during the experiment due, for example, to stick-slip phenomena, or if creep behaviour is present. To minimize, or better, eliminate this effect, lubrication would be needed.

4. Virtual Crack propagation

In the previous section, rubber envelope inflation was studied considering the two sets of boundary conditions encountered during the experiment. Theoretical equations were developed or calculating both the axisymmetric deformations and stresses in the rubber. In the current section, these equations are employed for calculation of the energy stored in the rubber during crack propagation. An energy balance equation is subsequently derived to evaluate the crack propagation condition in the frame of linear elastic fracture mechanics (LEFM) theory. Then, no large process zone is supposed to develop ahead the crack tip nor plastic deformation in the rubber envelope. Although LEFM is considered here, the process is expected to be highly nonlinear due to the material and geometrical nonlinearities. All possible additional dissipation mechanisms in the rubber due to viscosity or hardening are neglected at this stage.

4.1. Strain Energy Release Rate Evaluation

The entire test procedure is driven by injecting a pressurized fluid in between the rubber envelope and the steel cord. The overall energy balance can be described as follows. The energy input is due to the work done by the pressurized liquid. This becomes distributed

between the energy stored in the deformed rubber (and the small amount stored in the compressed fluid at high pressures) and that required to cause separation of the rubber / cord interface i.e. fracture energy. Once the initial liquid injection (system loading) is finished, the measured pressure remains reasonably constant during crack propagation (see *Figure 2* (a)). The process can therefore reasonably be assumed to be steady state and self-similar. In the following, a virtual crack extension 'δa' of the interface is considered along the cord. Due to the axial deformation, the additional length of free, unattached rubber is stretched to $\lambda_z \delta a$. The corresponding work done in pressure injection is then simply determined as the product of the constant pressure P_i at which the crack propagates and the injected fluid volume during the crack propagation:

$$W = P_i \pi (v^2 - v_0{}^2) \lambda_z \delta a \tag{15}$$

Taking into account the fluid compressibility constant 'χ', the potential energy stored in a compressible fluid during the crack propagation is given by relation:

$$E_{pf} = \frac{\pi}{2} \chi P_i{}^2 (v^2 - v_0{}^2) \lambda_z \delta a \tag{16}$$

In this analysis, the incompressible Mooney-Rivlin model is used to describe the mechanical behaviour of the rubber. The strain energy density of such a solid is given by the following relation:

$$\delta W(\lambda_z, \lambda_r, \lambda_\theta) = C_1 (I_1 - 3) + C_2 (I_2 - 3) \tag{17}$$

where:

$$I_1 = \lambda_z^2 + \lambda_r^2 + \lambda_\theta^2 \tag{18}$$

$$I_2 = \lambda_r^2 \lambda_z^2 + \lambda_\theta^2 \lambda_r^2 + \lambda_z^2 \lambda_\theta^2 \tag{19}$$

Therefore, the potential energy stored in the rubber per unit length is obtained by integrating the relation *(17)* over the tube cross-section as follows:

$$\delta E_{pr} = \int_{v}^{w} \delta W. 2\pi r dr \tag{20}$$

Using *(18)* and *(19)*, the above equation can be solved to obtain:

$$\delta E_{pr} = 2\pi \left[\frac{w^2 - v^2}{2} \left(C_1 \lambda_z{}^2 + 2C_1\lambda_z{}^{-1} + 2C_2\lambda_z + C_2\lambda_z{}^{-2} - 3C_1 - 3C_2 \right) \right.$$
$$\left. - \frac{C_1\lambda_z{}^{-1} + C_2\lambda_z}{c} \ln\left(\frac{w}{v}\right) - \frac{C_1\lambda_z{}^{-1} + C_2\lambda_z}{2c} \ln\left(\frac{cw^2 - 1}{cv^2 - 1}\right) \right] \tag{21}$$

It should be noted again that the integration is performed in the deformed state. Such procedure naturally takes into account the large displacement effects. Considering a virtual crack propagation of 'δa' along the cord, the deformation potential energy of the rubber tube is increased to $\lambda_z \delta a \delta E_{pr}$.

$$E_{pr} = 2\pi\lambda_z d\alpha \left[\{C_1(\lambda_z^2 + 2\lambda_z^{-1} - 3) + C_2(\lambda_z^{-2} + 2\lambda_z - 3)\} \left\{ \frac{w^2 - v^2}{2} \right\} \right.$$
$$\left. - \frac{C_1\lambda_z^{-1} + C_2\lambda_z}{c} \{\ln\left(\frac{w}{v}\right) - \frac{1}{2}\ln\left(\frac{cw^2 - 1}{cv^2 - 1}\right)\} \right] \tag{22}$$

Finally, the energy dissipated through the interfacial separation should be considered as given by the relation:

$$D = G_c. 2\pi v_0 \delta a \tag{23}$$

where, G_c is the critical SERR of the interface and $2\pi v_0 \delta a$ is the area of the fractured face.

Applying energy balance to the whole system:

$$W = E_{pf} + D + E_{pr} \tag{24}$$

The following expression of the critical strain energy release rate is found:

23

$$G = \frac{P_i(v^2 - v_0{}^2)\lambda_z}{2v_0} - \frac{\chi}{4v_0}P_i{}^2(v^2 - v_0{}^2)\lambda_z$$

$$- \frac{\lambda_z}{v_0}[\{C_1(\lambda_z^2 + 2\lambda_z^{-1} - 3) + C_2(\lambda_z^{-2} + \lambda_z - 3)\}\left\{\frac{w^2 - v^2}{2}\right\}$$

$$- \frac{C_1\lambda_z^{-1} + C_2\lambda_z}{c}\{ln\left(\frac{w}{v}\right) - \frac{1}{2}ln\left(\frac{cw^2 - 1}{cv^2 - 1}\right)\}]$$

$$(25)$$

In this expression, most of the terms are measurable quantities (Pi, λ_z, v, C_1, C_2, …) and/or are determined by solving the 'Rubber Tube Inflation Problem' from the measured inner pressure. The value of G does not depend on the initial crack length or debonding length which is consistent with the constant pressure measured. However, to avoid edge effects and to facilitate homogeneous inflation of the tube, an initial crack length of approx. *50%* of the total length of the specimen was chosen in the experimental test.

Depending on the rubber material properties, specimen dimensions, radial clearance for inflation ($= R - w_0$) and the strength of the interface, the crack propagation may occur during UIS or CIS. However, the method followed to calculate the energy balance is unchanged, therefore *Equation* (*25*) holds true in both cases.

Figure 11 shows the behaviour of the strain energy release rate – *Equation (25)* w.r.t. the fluid pressure during the crack propagation. A similar curve was also plotted using the FE model discussed previously. For the calculation of *G*, an approach similar to Virtual Crack Closure Technique (VCCT) was used. Five different crack lengths were modelled and specimen was inflated in the FE model up to the same maximum pressure. The difference in the energy stored in the models at any applied pressure gives the energy of fracture which along with corresponding crack length gives value of *G* at the specific pressure. Similar to previous results, again, the results from FE model and theoretical model match almost exactly.
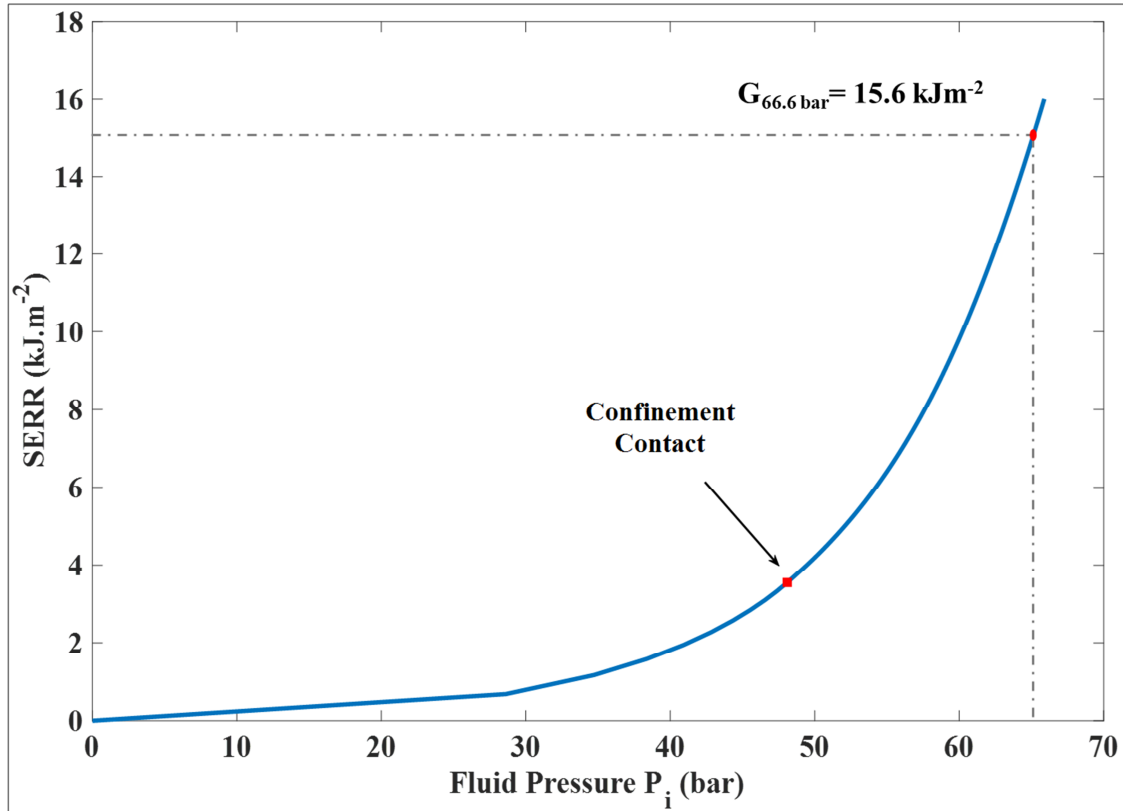
Figure 1: Strain Energy Release Rate as a function of injection Fluid Pressure.

The value of Gc (critical SERR) for the interface found by locating the crack propagation pressure observed during the experiment on the curve is 15.6 $kJ.m^{-2}$. The critical SERR obtained with an independent 90° peel test was 21.3 $kJ.m^{-2}$. A value of ~ 20$kJ.m^{-2}$ was found by (Fielding-Russell G. S.) in their peel tests. Although the values differ by a small amount, experimental conditions from the both tests should be adjusted to match the same loading rates and ageing conditions of the rubber and the interface. Such a detailed comparison would be interesting for future research prospects.

Using a VCCT-like approach, SERR was calculated from the FE model for 5 different crack lengths. The difference of energies stored in the system between two crack lengths was used to calculated energy of fracture and subsequently the SERR at given fluid pressure. *Figure 12* shows comparison of SERR calculated using *Equation (25)* and the VCCT-like FE approach.
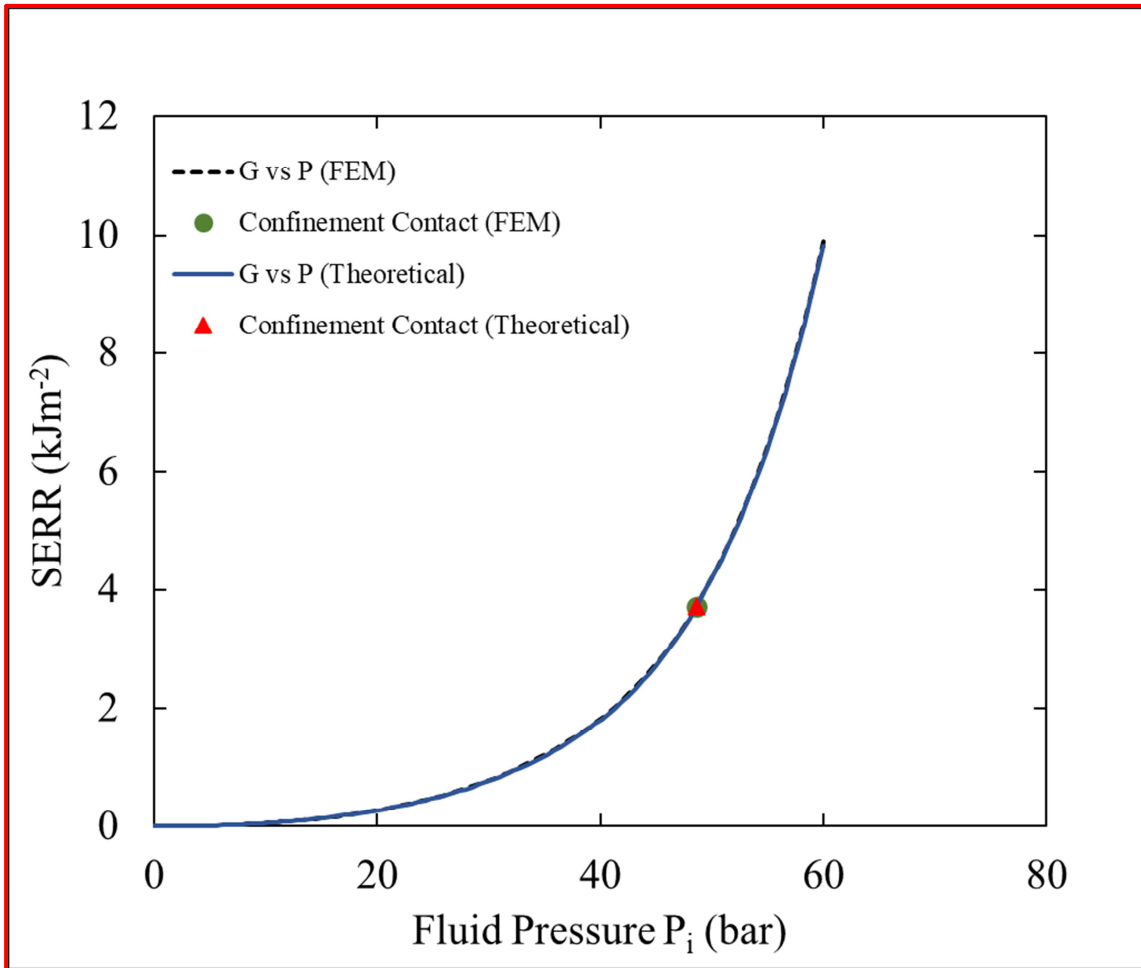
Figure 12: Evolution of SERR with applied pressure. Comparison between theoretical model and FE model.

It should be noted that, the calculation of G from (25) is valid only until the instability point as shown in *Figure 4*. Beyond the point P_{max} in *Figure 4*, as the fluid pressure begins dropping, the contribution of W in *Equation* (25) simultaneously begins to drop. However, the rubber envelope continues to store potential energy E_{pr} that gives a steadily decreasing value of G. To avoid such erroneous results, it is imperative to avoid the unstable inflation. A stable inflation prior to the crack propagation can be attained by reducing the ratio R/w_0, such that the CIS starts before the point $P_i=P_{max}$ is reached. The whole test can also be carried out under

purely CIS ($w_0=R$) which will certainly avoid the unstable inflation. However, the testing equipment should be designed to work under very high pressures.
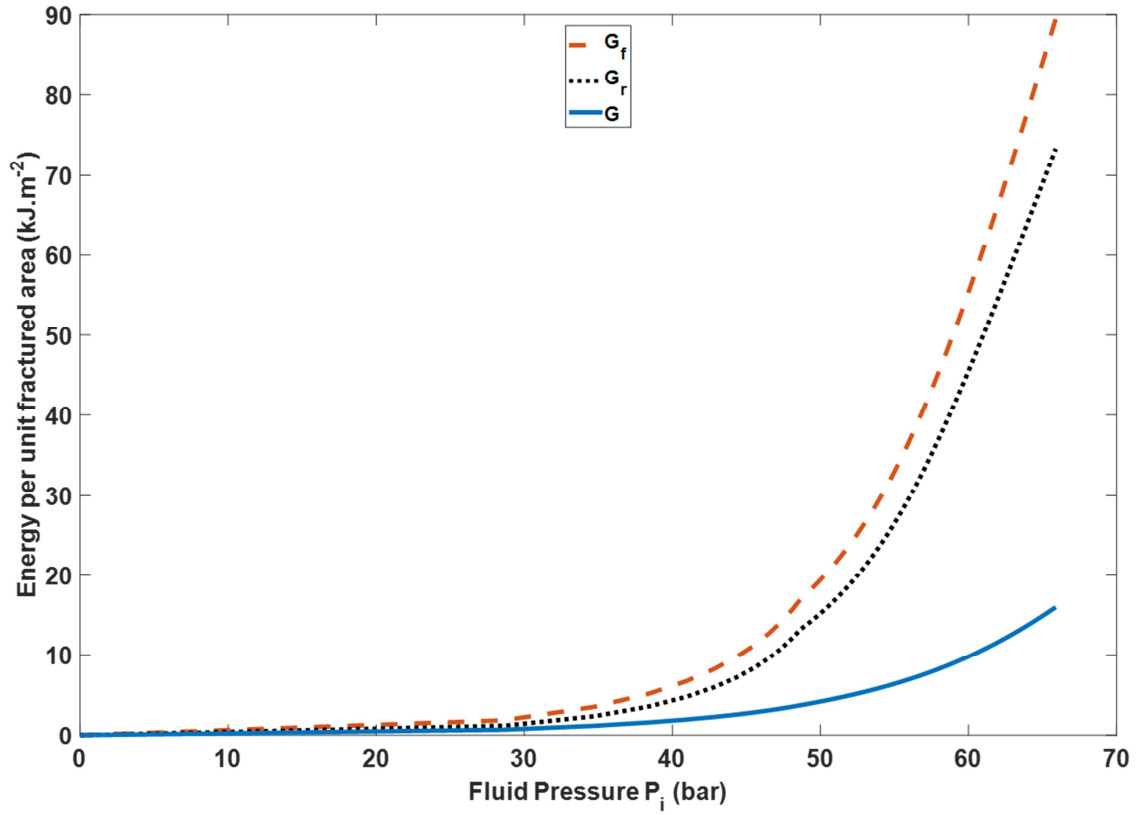

Figure 13: Comparison of the energies stored in the fluid and the rubber at crack propagation, calculated for a unit fractured area. G_r is the contribution of the rubber envelope and G_f is of the fluid.

A comparison of the contribution of the work needed for pressure injection (G_f) and that potential energy stored in the inflated rubber (G_r) w.r.t. the SERR (G) is shown in *Figure 13* for a unit fractured area. The contribution of the potential energy stored in the fluid compressibility is negligible ($<1\%$) for nearly incompressible fluids like pure water or seawater. The nonlinear behaviour of the function G can be explained by the nonlinear behaviour of rubber.

5. Conclusion

In the present article, a new test configuration is proposed to evaluate the fracture energy of a rubber/cord interface for tyre application. The test is a cylindrical version of the standard constrained blister test used to evaluate rubber adhesion on rigid substrates. The test procedure commences with injecting a fluid between the metal cord and a cylindrical rubber envelope. The pressure required to inflate the rubber envelope and to propagate the crack along the cord is measured during the experimental test. A mechanical analysis of this test is proposed here to evaluate the fracture energy from the measured pressure. Analytical modelling as well as numerical analyses are performed to take into account the incompressible hyperelastic nature and large deformation of the rubber envelope. The equations developed for the energy balance are strictly applied to an incompressible Mooney-Rivlin solid. However, the method followed can be applied to any nonlinear material if the strain energy density function (*Equation (17)*) and its relations with the Cauchy Stresses are known.

Due to the non-linear deformations, the determination of fracture is not straightforward since rigorous characterization of the rubber mechanical behaviour is needed. However, it is suggested that combining pressure monitoring with additional measurements such as longitudinal elongation of the rubber would enable a more direct evaluation of the critical SERR.

Further developments are still required at this step since the hypotheses made on the rubber mechanical behaviour are simple. In particular, following the analysis proposed on the more traditional rubber peel and blister tests, complementary analysis should be performed to evaluate the additional energy dissipation due to viscoelasticity and/or hardening during the crack propagation. The strain energy density function of the rubber can therefore be altered in

a way that the effects of loading rate on viscous dissipation can be taken into consideration during the system energy balance.

A rigorous study on the effect of various fluids on the crack propagation pressure as well as the fracture energy can be directly applied in the tyre industry. Since a fluid is used to inflate the rubber envelope, specimen-fluid interaction was observed during the tests (cord corrosion, rubber swelling etc.). These difficulties could be avoided by replacing the fluid (water) by other fluids (sqalene, mineral oil etc.). Besides, this also suggests that RCAIT could be of interest for quantitative characterization of rubber / cord durability as an alternative to the strip blister test (Hamadea R.F.).

This article focuses on the global evaluation of the total SERR that is facilitated by the self-similar nature of the crack propagation. However, a refined analysis of the transition zone is clearly of interest to evaluate the mode mixity condition as well as possible development of process zone ahead the crack tip. By coupling the pressure injection with an external axial load on the steel cord, a mixed mode crack propagation can be produced. Effect of mode mixing on the fracture energy can thus be studied by varying the proportions of the pressure and the external axial loads. Refined experimental and numerical mechanical analysis is required for precise evaluation of mode mixity condition at the crack tip, as observed in other configurations (Liechti K. M.), (Liechti et Adamjee), (Liechti K.M.), (Mauchien T. K.). This mode mixity will probably vary with the specimen and confinement tube dimensions therefore a parametric analysis is required in the future.

6. References

Anani Y., & Rahimi G.H. *Stress analysis of thick pressure vessel composed of functionally graded incompressible hyperelastic materials*. International Journal of Mechanical Sciences, 104, 1-7, 2015.

Brown R. *Physical Test Methods for Elastomers*. Springer Int. XIV-387, 2018.

Chang Y. S., Lai Y. H., & Dillard D. A. *The constrained blister—a nearly constant strain energy release rate test for adhesives*. The Journal of Adhesion, 27(4), 197-211, 1989.

Cook J. W., Edge S. & Packham D. E. *The adhesion of natural rubber to steel and the use of the peel test to study its nature*. International journal of adhesion and adhesives, 17(4), 333-337, 1997.

D1781-98(2012), ASTM. *Standard Test Method for Climbing Drum Peel for Adhesives*. ASTM International, West Conshohocken, PA, 2012.

D1871-04(2014), ASTM. *Standard Test Method for Adhesion Between Tire Bead Wire and Rubber*. ASTM International, West Conshohocken, PA, 2014.

D2229-10(2014), ASTM. *Standard Test Method for Adhesion Between Steel Tire Cords and Rubber*. ASTM International, West Conshohocken, PA, 2014.

D429-14, ASTM. *Standard test methods for rubber property – adhesion to rigid substrates*. ASTM International, West Conshohocken, PA, 2014.

Dannenberg H. *Measurement of Adhesion by a Blister Method*. Journal of Applied Polymer Science, 5 (14), 125-134, 1961.

Dillard D. A., Liechti K.M.,Lefebvre D. R., Lin C., Thornton J. S. & Brinson H. F. *Development of Alternative Techniques for Measuring the Fracture Toughness of Rubber-to-Metal Bonds in Harsh Environments*. ASTM, 1998.

Fielding-Russell G. S., Nicholson D. W. & Livingston D. L. *Physical Factors in Cord-to-Rubber Adhesion by a New Tire Cord Adhesion Test*. Tire Reinforcement and Tire Performance, ASTM, STP 694, 1979.

Gent A. N. *Elastic Instabilities in Rubber*. International Journal of Non-Linear Mechanics, 40 (2-3), 165-175, 2004.

Gent A.N., & Kaang S.Y. *Pull-Out and Push-Out Tests for Rubber-to Metal Adhesion*. Rubber chemistry and technology, 62(4), 757-766, 1989.

Hamadea R.F., Seifa C.Y., Dillard D.A. *Cathodic delamination of elastomer-to-metal adhesive joints: Experimental data and empirical modeling*. Int. J. Adhes. Adhes. 27(2), 108-121, 2007.

Jamshidi M., Afshar F., Mohammadi N., & Pourmahdian S. *Study on cord/rubber interface at elevated temperatures by H-pull test method*. Applied surface science, 249(1-4), 208-215, 2005.

Lechtenboehmer A., Moneypenny H. G. & Mersch F. *A review of polymer interfaces in tyre technology*. Polymer International, 22(4), 265-301., 1990.

Liechti K. M., Becker E.B., Lin C. & Miller T.H. *A fracture-analysis of cathodic delamination in rubber to metal bonds*. Int. J. Fract. 39(1-3): p. 217-234., 1989.

Liechti K.M., Wu, J.D. *Mixed-mode, time-dependent rubber/metal debonding*. J. Mech. Phy. Solids, 49(5): p. 1039-1072., 2001.

Liechti, K. M. and W. Adamjee. *Mixed-mode cathodic delamination of rubber from steel*. J. Adhes., 40(1): p. 27-45., 1992.

Mauchien T. K., Liechti, K. M. *A fracture analysis of cathodic delamination at polyurea/steel interfaces*. Int. J. Adhes. Adhes. 51(0): p. 23-31., 2014.

Mooney M. *A Theory of Large Elastic Deformation*. Journal of Applied Physics, 11, 582, 1940.

Napolitano M.J., Chudnovsky A., Moet A. *The constrained blister test for the energy of interfacial adhesion*. Journal of Adhesive Science and Technology, 2:1, 311-323, 1988.

Parsons M., Polyakova A., Stepanov E. V., Hiltner A. & Baer E. *Evaluation of the constrained blister test for measuring adhesion*. The Journal of Adhesion, 68(1-2), 45-63, 1998.

Rault V., Vignal V., Krawiec H. & Tadjoa O. *Corrosion behaviour of heavily deformed pearlitic and brass-coated pearlitic steels in sodium chloride solutions*. Corrosion Science, 86, 275-284., 2014.

Skala D. P. *Modified Equations of Rubber Elasticity Applied to The Inflation Mechanics of A Thick-Walled Rubber Cylinder*. Rubber Chemistry and Technology, 43 (4), 745-757, 1970.

Stevenson A. *On the durability of rubber/metal bonds in seawater*. International journal of adhesion and adhesives, 5(2), 81-91, 1985.

van Ooij, W. J. *The role of XPS in the study and understanding of Rubber-to-metal bonding*. Surface Sci. 68(1977)1, 1977.

Vignal V., Rault V., Krawiec H., Lukaszczyk A. & Dufour F. *Microstructure and corrosion behaviour of deformed pearlitic and brass-coated pearlitic steels in sodium chloride solution*. Electrochimica Acta, 203, 416-425., 2016.

Zelin M. *Microstructure evolution in pearlitic steels during wire drawing*. Acta Materialia, 50(17), 4431-4447., 2002.